Large-Scale Triaxial Experiments on the Creep Behavior of a Saturated Rockfill Material

Zhongzhi Fu[1]; Shengshui Chen[2]; and Beixiao Shi[3]

Abstract: Large-scale triaxial compression and creep experiments were conducted with a saturated limestone rockfill material. The relationships between dilatancy ratio and stress ratio during loading and creeping were analyzed. It was found that the dilatancy ratio during both loading and creeping decreased nonlinearly when the stress ratio increased. In addition, the positive dilatancy ratio was considerably higher in creep than in vertical loading under the same stress state. Experimental data also showed that creep strains evolve linearly with the logarithm of time after a certain period, and both the final amounts of creep strains at the end of experiments and their rates are influenced by the stress states. A higher confining pressure and higher deviatoric stress lead to larger creep strains and higher strain rates. Empirical equations relating the final amounts of creep strains and their rates to the stress states are suggested. **DOI: 10.1061/(ASCE)GT.1943-5606.0001898.**

Author keywords: Rockfill material; Triaxial experiment; Creep; Plastic flow; Dilatancy.

Introduction

It is widely recognized that the deformation of rockfill dams may last several years after dam construction and reservoir impounding (Clements 1984; Oldecop and Alonso 2007). Particle breakage under highly concentrated contacting stresses and environmental variation is widely thought to be the main reason for this long-term behavior (Oldecop and Alonso 2007; Kwok and Bolton 2013; Fu et al. 2012). Practice in rockfill dam engineering shows that excessive postconstruction deformation may result in damage to impermeable systems, and consequently potentially threaten the safety and operability of relevant projects (Zhang et al. 2004). It is, therefore, of great significance to make a reliable prediction of the long-term deformation of rockfill dams during the design stage.

Early efforts have been made, on the basis of available field observations, to establish some empirical formulas expressing the crest settlement as a function of dam height and other factors (Clements 1984; Hunter and Fell 2003). However, the applicability of these models is generally limited due to the uniqueness of each particular project. Crest settlement in itself cannot give any indication of the performance or safety of impermeable systems. With the progresses in experimental techniques and computational methods, increasing efforts are now being spent in developing advanced creep models using various constitutive frameworks (Oldecop and Alonso 2001; Dolezalova and Hladik 2011; Alonso et al. 2005; Fu et al. 2012). These models can be used in certain numerical procedures to predict the long-term deformation of rockfill dams, and the reliability of such a prediction largely depends on the model used and the corresponding parameters. Creep experiments unquestionably play a central role in model calibration and parameter identification.

Compared with the vast amounts of static loading experiments conducted with a variety of rockfill materials (Charles and Watts 1980; Indraratna et al. 1993; Yasuda and Matsumoto 1994; Varadarajan et al. 2003; Ovalle et al. 2015; Xiao et al. 2014a, b, 2016a, b), experimental studies on their time-dependent deformation behavior under constant stress states (after loading) are considerably less abundant. The long testing time required and the technical difficulties in sustaining stable stress states in laboratory may be the most important reasons (Kuwano and Jardine 2002). Cheng and Ding (2004) are among the few authors who conducted a series of large-scale load-controlled creep experiments on a kind of limestone. The diameter and height of cylindrical specimens were 300 and 600 mm, respectively. It was found that the amounts of creep strains, including axial strain and volumetric strain, could be expressed as power functions of the elapsed time. Empirical equations describing the relationships between the final amounts of creep strains at the end of creep experiments and the stress states were also established (Cheng and Ding 2004).

Recently, the coupling effect between loading and creep was studied by Zhang et al. (2017) with a weathered granite. It was found that creep strains under constant stress states can also result in plastic hardening of rockfill materials. Loading after a creep process is initially in the elastic regime until the creep-altered yield surface is reached again, and henceforth, the material undergoes elastoplastic loading, following approximately the stress–strain curves of materials without any creep histories. Similar creep-induced stiffening has also been observed in various sands (Lade and Liu 1998; Lade et al. 2009; Karimpour and Lade 2010, 2013). It was interpreted that creep-induced structuration, which is defined as outward movement of the yield surface location as a result of the change in grain configuration and interlocking during creeping, has to be overcome to produce further plastic strains (Lade et al. 2009; Karimpour and Lade 2013). Another important finding from creep experiments with Antelope Valley sand (Lade and Liu 1998) and Virginia Beach sand (Karimpour and Lade 2010,

[1]Senior Engineer, Dept. of Geotechnical Engineering, Nanjing Hydraulic Research Institute, 34 Hujuguan Rd., Nanjing 210024, China (corresponding author). Email: fu_zhongzhi@yahoo.com

[2]Professor, Key Laboratory of Failure Mechanism and Safety Control Techniques of Earth-Rock Dams, Ministry of Water Resource, 223 Guangzhou Rd., Nanjing 210029, China. Email: sschen@nhri.cn

[3]Senior Engineer, Dept. of Geotechnical Engineering, Nanjing Hydraulic Research Institute, 34 Hujuguan Rd., Nanjing 210024, China. Email: bxshi@nhri.cn

Note. This manuscript was submitted on June 20, 2017; approved on January 10, 2018; published online on May 3, 2018. Discussion period open until October 3, 2018; separate discussions must be submitted for individual papers. This paper is part of the ***Journal of Geotechnical and Geoenvironmental Engineering***, © ASCE, ISSN 1090-0241.

2013) is that the volume change curves corresponding to creep stages do not deviate from the reference curves obtained from loading experiments, indicating that the direction of inelastic creep strain increments is the same as that of the plastic strain increments. That is to say, an identical potential function may be used to evaluate the directions of inelastic creep and plastic strains simultaneously. However, this assumption was invalidated in creep experiments with Carib Sea Geomarine Florida crushed coral sand (Lade et al. 2009), which is more friable compared with previously mentioned ones.

Excavated rockfill materials are also prone to particle breakage during loading and creeping due to the presence of abundant sharp corners and microcracks (Indraratna et al. 1993; Tapias et al. 2015; Oldecop and Alonso 2007; Xiao et al. 2016b), and it may be inferred that the direction of creep strains does not necessarily coincide with that of loading-induced plastic strains, such as in friable coral sand. This is a fundamental issue that should be clarified before establishing creep models. In this study, a series of large-scale triaxial compression and creep experiments were conducted with an excavated rockfill. The stress–dilatancy characteristics during loading and creeping were studied and compared in order to elucidate the aforementioned point. The dependence of the final amounts of creep strains at the end of experiments and their evolution processes upon the stress states were also studied. Throughout the paper, compressive stresses and strains are defined as positive in accord with the sign convention in soil mechanics. In addition, all the normal stresses are effective ones and the conventional comma is omitted for simplicity.

Apparatus and Tested Materials

Testing Apparatus

Both triaxial compression and creep experiments were performed with a large-scale triaxial testing apparatus. The equipment allows testing cylindrical specimens with diameters of 10, 20, and 30 cm. A maximum confining pressure of 4 MPa can be applied, and the maximum axial force achievable is 1,500 kN, accounting for a maximum deviatoric stress of approximately 21 MPa for largest specimens. The controlling precision of the axial force and confining pressure are 0.05 kN and 0.1 kPa, respectively. A traditional deformation measurement system is used in this apparatus, i.e., axial strain is measured by a dial gauge mounted to the loading piston and the volumetric strain by recording the volume of water expelled from or sucked into specimens. The measurement precision of axial displacement and volume change are 0.001 mm and 0.1 mL, respectively. Lade and Liu (1998) proved that such a traditional measurement system can also yield satisfactory results comparable to those obtained with local strain monitoring techniques. To minimize the possible influence of temperature variation (Kuwano and Jardine 2002; Mitchell and Soga 2014), central air-conditioning was used during all the experiments, keeping the temperature in the laboratory at 15 ± 0.5°C.

Tested Materials

Rockfill excavated from a local material site for a concrete face rockfill dam was used in the experimental program. The material is mainly composed of limestone, with the largest particles of approximately 0.5 m in diameter. The average uniaxial compressive strengths of natural and saturated rock specimens are 84.9 and 77.4 MPa, respectively, indicating a hard-rock nature of the rockfill particles.

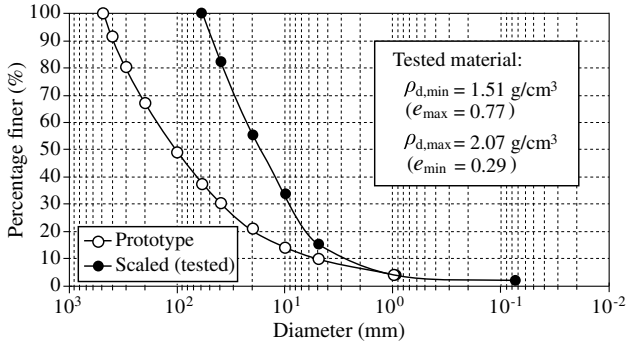

Fig. 1. Grain-size distributions of the prototype and tested material.

Due to the size limitation of the testing apparatus, the prototype material should be scaled down using the parallel grading method, particle replacing method, or a combination of both. Previous studies showed that to minimize the scale effect, the diameter of specimens should be at least 5–6 times larger than the largest particles (Marachi 1969). That is to say, for specimens with a diameter of 30 cm, the largest particles allowed is 5–6 cm in diameter. In this study, the prototype material was first scaled down using the parallel grading method (scaled-down ratio of 2.4); then, the yet-oversized particles were replaced by smaller ones. Fig. 1 shows the grain-size distributions of the prototype and scaled (tested) materials. The minimum dry density $\rho_{d,\min}$ and maximum dry density $\rho_{d,\max}$ as well as the corresponding characteristic void ratios, are also included in the figure.

The scale effect in laboratory testing of coarse granular materials is still an open issue in the geotechnical discipline. Most previous studies focused on the scale effect on the shear strength of tested materials (Marachi 1969; Frossard et al. 2012; Xiao et al. 2014c), and its influence on their deformation properties was rarely clarified and quantified. Some super-large-scale triaxial apparatuses developed around the world (Hu et al. 2011), usually allowing a maximum specimen diameter of 1 m, may provide new tools to shed light on this long-standing issue. Herein, the scale effect is not considered, and the scaled material is thought to be a satisfactory representative of the coarser prototype.

Experimental Procedures

Preparation of Samples

The oversized particles were first crushed to smaller ones. Then, the crushed material was sieved into six groups, i.e., 40–60 mm, 20–40 mm, 10–20 mm, 5–10 mm, 1–5 mm, and 0–1 mm. The total mass of each specimen was calculated according to the specimen size (30×70 cm) and objective dry density ($\rho_d = 1.95$ g/cm^3), and the proper mass of the material was fetched from each group and mixed together fully according to the objective grading. This mixed rockfill was filled in five equal portions into a steel mold that was tightly embraced by a cylindrical membrane (2.5 mm) from inside.

To achieve the designed dry density, a vibrator with a frequency of 40 Hz was used to densify the rockfill after the filling of each portion. A rubber pad (5 mm) was placed between the vibrator and those surface particles so as to avoid rigid contacts, therefore minimizing the particle breakage that may occur during compaction (Alonso et al. 2016). After the filling and compaction of all five portions, a porous disk and a specimen cap were placed on the top of the specimen, and then the steel mold was removed. The

rubber membrane used in this study was thick enough that it can be considered impermeable even in the long-term creep experiments. Therefore, leakage through the membrane as mentioned by Lade and Liu (1998) was considered impossible. However, the membrane may be punctured by particles with sharp corners under a high confining pressure. Therefore, adhesive tape was stretched to surround the prepared specimens as a protective measure.

Testing Procedures

After preparing an acceptable specimen, a high-strength steel chamber was installed and the specimen was submerged within the cell. In order to ensure the stability of the specimen, a confining pressure of 35 kPa was applied before saturating and testing. Then, a small magnitude of backpressure (30 kPa) was applied, and the specimen was saturated by deaired water from its bottom for 24 h. The measured pore-pressure parameter B was generally higher than 0.95 after the saturation process.

Conventional drained triaxial compression experiments were performed under four different levels of confining pressure, i.e., $\sigma_3 = 300$, 600, 900, and 1,200 kPa, and the vertical load was applied in a strain-driven mode. After application of the confining pressure, axial displacement was applied to the bottom of the tested specimen at a rate of 2 mm/min until shear failure occurred or the axial strain achieved a magnitude of 15%. The axial load and displacement as well as the volume of water expelled from or sucked into the specimen were registered. In particular, the peak deviatoric stress $(\sigma_1 - \sigma_3)_f$ under each confining pressure was recorded to design the deviatoric stresses under which creep experiments were performed.

Drained triaxial creep experiments were conducted under the same levels of confining pressure, and under each confining pressure, four levels of deviatoric stress were set, i.e., $(\sigma_1 - \sigma_3)/(\sigma_1 - \sigma_3)_f = 0.0$, 0.2, 0.4, and 0.8. The axial load was calculated according to the designed deviatoric stress level and was applied in a load-driven mode in creep experiments. After the application of the confining pressure and the axial load, they were kept constant over the following days, and the axial displacement as well as the volume change of the tested specimen were recorded. A total of 16 specimens were tested in creep experiments, and each experiment was terminated when the incremental axial strain during 24 h was less than 5×10^{-5}.

Experimental Results and Interpretations

Stress Dilatancy Characteristics during Loading

Similar to previous findings (Charles and Watts 1980; Indraratna et al. 1993; Varadarajan et al. 2003; Xiao et al. 2014b; Alonso et al. 2016), the tested rockfill exhibited a higher initial tangential modulus and higher peak deviatoric stress under a higher confining pressure. Shear dilation following an initial contraction could be observed under all four confining pressures, and the maximum volume contraction also increased with an increase in confining pressure.

To separate the elastic and plastic strains from the total ones, the following power function (Fu et al. 2014) was used to evaluate the elastic modulus, E_e, for a given confining pressure:

$$E_e = k_e \cdot p_a \cdot \left(\frac{\sigma_3}{p_a}\right)^n \tag{1}$$

where p_a = atmospheric pressure (≈101.325 kPa); and k_e and n = parameters. For the tested rockfill, $k_e = 2{,}200$ and $n = 0.20$. Furthermore, the value of Poisson ratio (ν) was set to 0.3 in strain separation.

Fig. 2 shows typical relationships between the dilatancy ratio, d, and stress ratio, η. The dilatancy ratio, d, is defined as the ratio between the incremental plastic volumetric strain, $d\varepsilon_v^p$, and incremental plastic deviatoric strain, $d\varepsilon_s^p$, that is

$$d = \frac{d\varepsilon_v^p}{d\varepsilon_s^p} \tag{2}$$

In triaxial experiments, the incremental plastic strains can be calculated using the axial plastic strain increment, $d\varepsilon_1^p$, and horizontal plastic strain increment, $d\varepsilon_3^p$, as follows (Been and Jefferies 2004; Li and Dafalias 2000):

$$d\varepsilon_v^p = d\varepsilon_1^p + 2d\varepsilon_3^p \tag{3a}$$

$$d\varepsilon_s^p = \frac{2}{3}(d\varepsilon_1^p - d\varepsilon_3^p) \tag{3b}$$

The stress ratio, η, in Fig. 2 is defined as the ratio between deviatoric stress, q, and mean effective stress, p

$$\eta = \frac{q}{p} \tag{4}$$

in which the particular expressions of the two stress invariants in triaxial experiments are given as follows (Been and Jefferies 2004; Li and Dafalias 2000):

$$p = \frac{1}{3}(\sigma_1 + 2\sigma_3) \tag{5a}$$

$$q = \sigma_1 - \sigma_3 \tag{5b}$$

where σ_1 and σ_3 = vertical stress and horizontal stress, respectively.

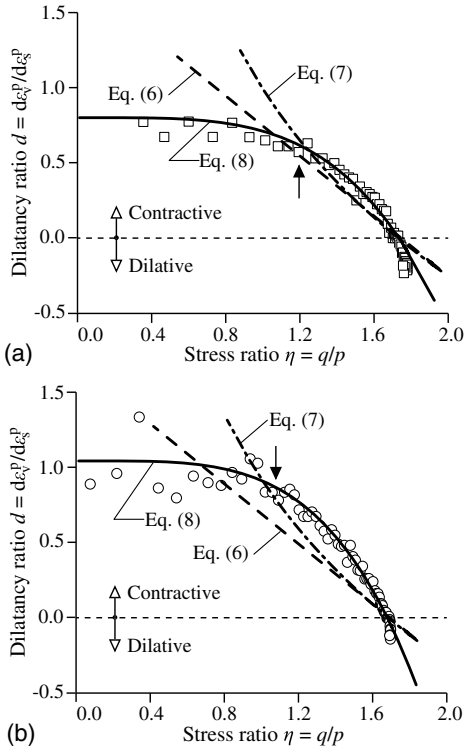

Fig. 2. Typical relationships between dilatancy ratio and stress ratio: (a) $\sigma_3 = 600$ kPa; and (b) $\sigma_3 = 1{,}200$ kPa.

It can be seen in Fig. 2 that the experimental data (open circles) concentrate rather well along narrow bands when the stress ratio is higher than 0.8. However, data scatterness can be seen when the stress ratio is lower than this threshold. A similar phenomenon has also been observed when interpreting the dilatancy behavior of sands and gravels (Pradhan et al. 1989; Been and Jefferies 2004; Kong et al. 2016), and it was thought to be the effect of initial fabric (Been and Jefferies 2004). Another possible source is the bedding error introduced at both ends of specimens (Jardine et al. 1984; Scholey et al. 1995; Clayton 2011), which is difficult to avoid in testing coarse aggregate materials. To avoid unreasonable data fluctuations, some of the experimental results at the very beginning of axial loading were abandoned, but the overall trends of the data were not altered. The remaining data points show that the dilatancy ratio decreases slowly from a certain positive value when the stress ratio is increased from zero until a certain threshold, which is marked by solid arrows in Fig. 2. After that, the decreasing rate increases until a negative dilatancy ratio is attained, indicating the occurrence of plastic volume expansion.

Many stress dilatancy equations have been proposed in the past (Schofiled and Wroth 1968; Roscoe and Burland 1968; Li and Dafalias 2000; Been and Jefferies 2004; Alonso et al. 2016; Xiao et al. 2016a) and the most well-known ones are probable the relation used in the Cam-clay model (Schofiled and Wroth 1968)

$$d = M_c - \eta \tag{6}$$

and the one used in the modified Cam-clay model (Roscoe and Burland 1968)

$$d = \frac{M_c^2 - \eta^2}{2\eta} \tag{7}$$

where M_c = constant volume stress ratio, and it is generally related to the critical state friction angle (Schofiled and Wroth 1968). M_c can also be evaluated using stresses at the instants of maximum volumetric strains (Fu et al. 2014). Herein, the latter way was used because critical states were never achieved in the current experiments. Although both Eqs. (6) and (7) have been widely used in constitutive models, their suitability in modeling the deformation behavior of the tested rockfill is limited, as can be seen in Fig. 2, particularly for the one given by Eq. (7). Been and Jefferies (2004) also found that an inconsistent trend was predicted by Eq. (7) in modeling the stress dilatancy behavior of a loose sand. The original linear relation given by Eq. (6) is also not an acceptable approximation herein. Both equations overestimate the positive dilatancy ratio when the stress ratio is relatively low.

By trying different forms of alternative stress dilatancy equations, it was found that the following nonlinear power function is a good choice that can reproduce well the experimental data, especially when the dilatancy ratio is positive:

$$\frac{d\varepsilon_v^p}{d\varepsilon_s^p} = d_0\left[1 - \left(\frac{\eta}{M_c}\right)^4\right] \tag{8}$$

where d_0 = initial dilatancy ratio under isotropic stress states, and geometrically it is the intercept of the approximating curve upon the ordinate ($\eta = 0$). Fig. 2 shows the satisfactory agreement between the curves made by Eq. (8) and the corresponding experimental results. In the following part, Eq. (8) was used as a reference in studying the creep strain direction.

Table 1 gives the values of the two parameters in Eq. (8), i.e., d_0 and M_c, for different confining pressures. The initial dilatancy ratio increases with the confining pressure, whereas the constant volume stress ratio follows an opposite trend. Decreases in the constant-volume stress ratio under triaxial stress states have been noticed previously (Fu et al. 2014). Xiao et al. (2014a, 2016a) also found, in a series of true triaxial experiments with typical rockfills, that the constant-volume friction angle decreases with an increase in the minor principal stress at any given intermediate principal stress ratio [$b = (\sigma_2 - \sigma_3)/(\sigma_1 - \sigma_3)$].

The influence of confining pressure on the initial dilatancy ratio is twofold. On one hand, increasing the confining pressure results in an increase of contacting forces between particles and may give rise to enhanced particle abrasion and breakage during shearing. On the other hand, a higher confining pressure also means a more compacted fabric and higher average coordination number of particles prior to shearing. This is an opposing factor that may reduce the void available for contraction as well as reduce the contacting forces. The increasing trend in Table 1 indicates, however, that the first effect predominates.

Furthermore, plotting the dilatancy ratio against the stress ratio results in densely overlapped experimental data for negative dilatancy stages (Fig. 2), and Eq. (8) is not equivalently effective in interpreting these segments of data. More sophisticated stress dilatancy theories (e.g., Li and Dafalias 2000; Alonso et al. 2016) may be used. For instance, Alonso et al. (2016) recently suggested incorporating the plastic work in constructing a stress dilatancy equation for rockfill materials.

Viscoplastic Flow Direction during Creeping

Creep experiments were conducted under constant stress states, and all the strains developed are essentially plastic. Therefore, the term viscoplastic is used here to describe the time-dependent creep strains. Fig. 3 shows the accumulation of the axial strain and volumetric strain during creeping (solid curves) obtained under the confining pressures of 0.6 and 1.2 MPa. The experimental results obtained in triaxial compression experiments are also overlapped in this figure (dashed curves) for comparison.

Two general features can be observed in Fig. 3. First, the amount of axial creep strain is larger when the deviatoric stress is higher for a given confining pressure, as also found by others (Cheng and Ding 2004; Kwok and Bolton 2013; Zhang et al. 2017). Second, the volumetric strains during creeping do not follow the same paths obtained in vertical shearing. Evident deviation of the creep paths from the primary loading curves (ε_v versus ε_1) can be seen in all stress states, and the creep-induced volumetric strains are considerably more contractive than the loading-induced ones. That is to say, the plastic potential function used to determine the direction of plastic strains during loading may not be used equivalently to determine the viscoplastic flow direction during creeping. More contractive behavior during creeping was also found in a crushed coral sand (Lade et al. 2009) and a slightly weathered granite rockfill (Zhang et al. 2017). A similar suggestion of devising a different potential function for creep strains was proposed by Lade et al. (2009).

Table 1. Dependence of the parameters d_0 and M_c (M_c') on the confining pressure σ_3

σ_3 (kPa)	d_0	M_c	M_c'	M_c'/M_c
300	0.75	1.89	2.14	1.13
600	0.80	1.74	2.09	1.20
900	1.00	1.69	2.03	1.20
1,200	1.05	1.68	2.01	1.20

J. Geotech. Geoenviron. Eng., 2018, 144(7): 04018039

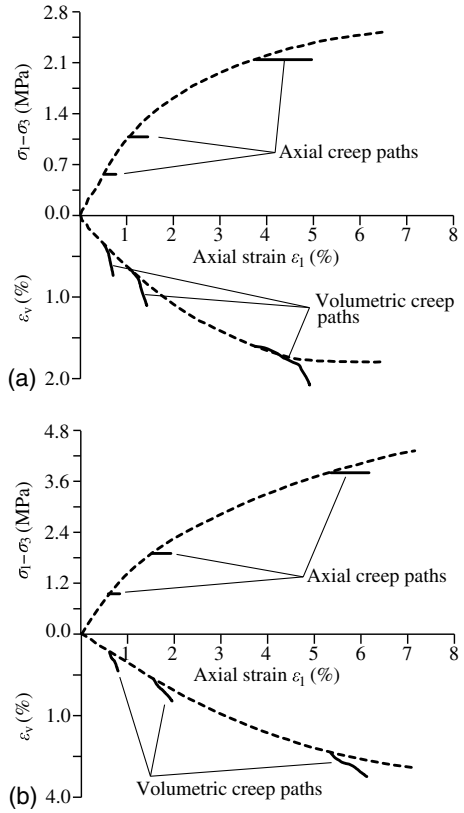

Fig. 3. Typical creep paths under different deviatoric stresses: (a) $\sigma_3 = 600$ kPa; and (b) $\sigma_3 = 1{,}200$ kPa.

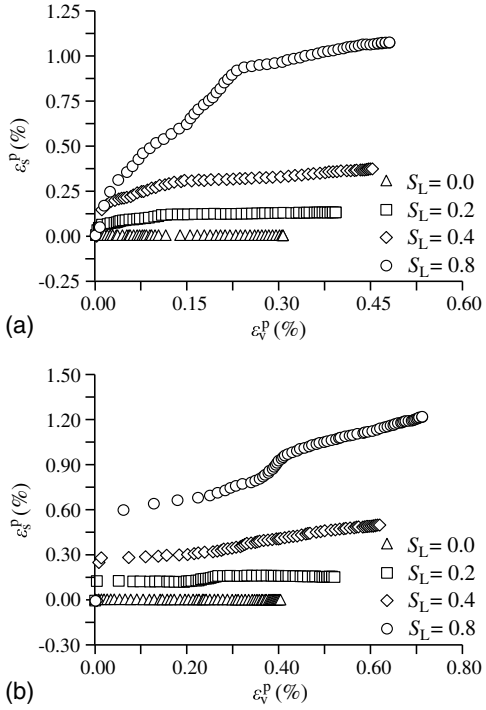

Fig. 4. Deviatoric strain versus volumetric strain during creeping: (a) $\sigma_3 = 600$ kPa; and (b) $\sigma_3 = 1{,}200$ kPa.

A closer inspection of the creep paths on the ε_v versus ε_1 plane reveals another important fact. The direction of creep strains evolves continuously, and it does not necessarily remain constant during creeping. This phenomenon can be more clearly seen in Fig. 4, in which the creep paths under different deviatoric stress levels $[S_L = (\sigma_1 - \sigma_3)/(\sigma_1 - \sigma_3)_f]$ were converted onto the ε_s versus ε_v plane. The following observations deserve to be mentioned:

- Under isotropic stress states ($S_L = 0$), small negative deviatoric strains ($\varepsilon_1 < \varepsilon_3$) developed, indicating a stiffer response of the tested specimens to vertical loading than to radial loading. This stiffness anisotropy may be caused by the preparation method of specimens and can lead to radial strains exceeding the axial strains (Kuwano and Jardine 2002). However, the magnitudes of the deviatoric strains are always negligible compared with those of the volumetric strains, indicating that the stiffness anisotropy after applying the confining pressure is not evident and negligible.
- Under anisotropic stress states, abrupt increases or jumps of deviatoric strains can almost always be observed at the beginning of creeping. The amounts of deviatoric strains developed during the first few minutes can be large portions of the final amounts. The volumetric strains, on the other hand, always accumulate in a gradual way without visible sudden increases. In this study, creep strains were always measured 10 min after the objective vertical stresses were achieved, and it is possible that the measured quantities at the very beginning include some loading-induced parts. There is no criterion for creep experiments specifying the end of loading-induced deformation and the initiation of creep strains.

The sudden increase of deviatoric strains and evolving direction of creep strains described in preceding paragraphs pose difficulties in establishing a viscoplastic flow rule for creep in an incremental manner. However, it may be interesting to study the influence of the stress level on the average creep dilatancy ratio, defined herein as the ratio between the final creep volumetric strain and final deviatoric creep strain

$$d_c = \frac{\varepsilon_v^f}{\varepsilon_s^f} \tag{9}$$

where d_c = creep dilatancy ratio; and ε_v^f and ε_s^f = final amounts of volumetric creep strain and deviatoric creep strain, respectively. The term final is used here to signify the creep strains accumulated until the end of experiments.

Fig. 5 shows the dependence of the creep dilatancy ratio on the stress ratio as represented by the solid asterisks. The values of d_c under isotropic stress states ($\eta = 0$) tend to infinity and were not included here due to the scale of the ordinate. The stress dilatancy relations given by Eq. (8) were also plotted in this figure for comparison. It is clear that the specimens exhibit evident volume contraction when the stress ratio is relatively low, and the creep dilatancy ratio decreases when the stress ratio is increased. For any stress states, Eq. (8) underestimates the volume contraction considerably, and it is a strong evidence that the flow rule during loading is not appropriate for creeping. The data trends can neither be modeled by the linear relation given by Eq. (6).

Considering the fact that $d_c \to \infty$ when $\eta \to 0$ and the data trends shown in Fig. 6, it may be suitable to use Eq. (7) to represent the dependence of d_c upon η. A data-fitting process validated this postulation, as shown by the agreement of the experimental data and the dashed curves. However, the constant volume stress ratio, M_c', used in constructing the dashed curves are different from M_c determined from triaxial compression experiments. For a given confining pressure, the value of M_c' is slightly higher than that of M_c, as indicated in Table 1. A rough estimation may be given by $M_c' \approx (1.10 - 1.20)M_c$. That is to say, if a creep experiment is performed under a stress ratio higher than M_c but lower than M_c',

J. Geotech. Geoenviron. Eng., 2018, 144(7): 04018039

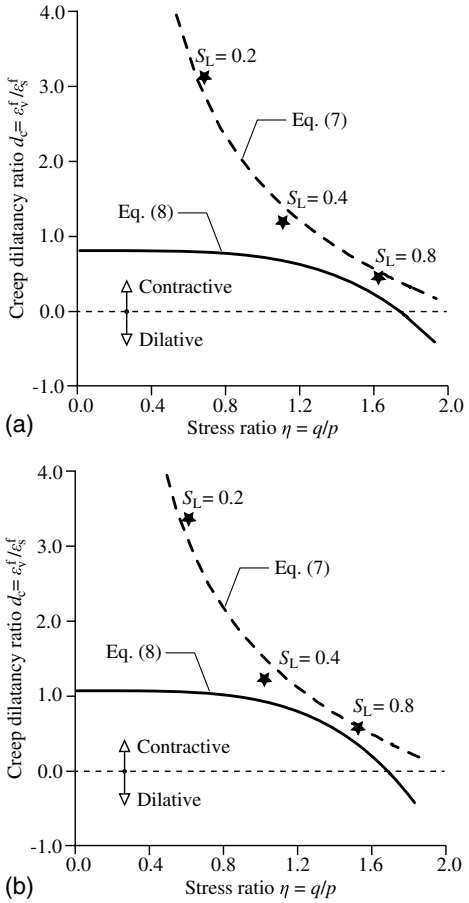

Fig. 5. Typical relationships between creep dilatancy ratio and stress ratio: (a) $\sigma_3 = 600$ kPa; and (b) $\sigma_3 = 1{,}200$ kPa.

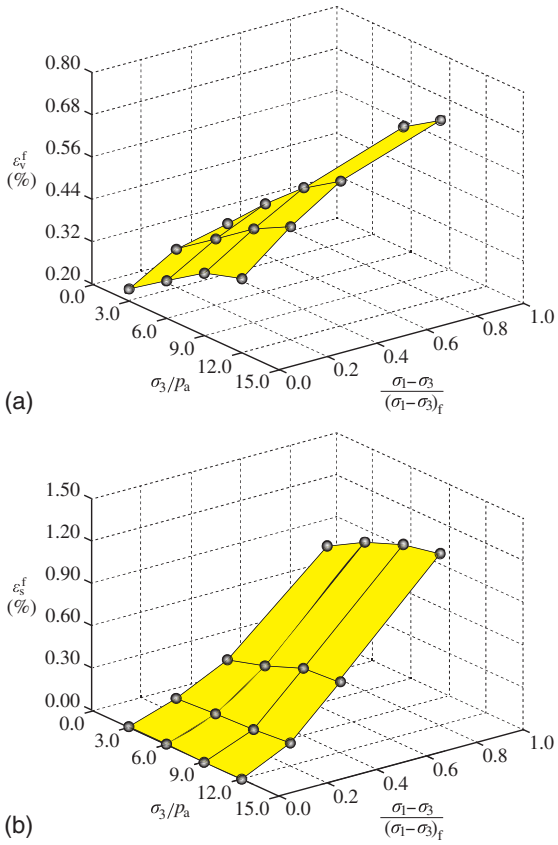

Fig. 6. Dependence of the final amounts of creep strains on the stress states: (a) volumetric creep strain; and (b) deviatoric creep strain.

volume contraction will occur during creeping, whereas dilation occurs if axial loading does not cease. It is also possible that M_c' is even higher than the peak stress ratio (M_f) of the tested material. In this case, Eq. (7) will always predict a volume contraction during creeping. Lade et al. (2009) suggested that a potential for creep strains should indicate contraction at every stress point for their tested coral sand.

Final Amounts of Creep Strains

Table 2 lists the final amounts of creep strains measured at the end of all 16 creep experiments. The second and third rows are deviatoric stresses at the peak states in triaxial compression experiments and the corresponding stress ratios obtained.

The final amounts of creep strains are plotted against the confining pressure and stress level in Fig. 6. Both the volumetric strain and deviatoric strain show dependence on the confining pressure and stress level. For a given confining pressure, the volumetric strain and deviatoric strain increase when the stress level is enhanced. Similarly, for a given stress level, a higher confining pressure also results in larger creep strains (ε_v^f and ε_s^f). Some empirical models expressing the final amounts of creep strains as functions of stress quantities have been proposed previously (Cheng and Ding 2004; Zhang et al. 2004; Zhou et al. 2011). Herein, an alternative choice is provided for the evaluation of creep strains

$$\varepsilon_v^f = c_1 \left(\frac{p}{p_a}\right)^{n_1} + c_2 \left(\frac{q}{p_a}\right)^{n_2} \tag{10a}$$

Table 2. Final amounts of creep strains at the end of experiments

σ_3 (kPa)	$(\sigma_1-\sigma_3)_f$ (kPa)	M_f	$\frac{\sigma_1-\sigma_3}{(\sigma_1-\sigma_3)_f}$	η	ε_v^f (%)	ε_s^f (%)
300	1,653	1.94	0.00	0.00	0.231	0.000
			0.20	0.81	0.307	0.114
			0.40	1.27	0.336	0.276
			0.80	1.79	0.376	0.905
600	2,657	1.79	0.00	0.00	0.307	0.000
			0.20	0.68	0.389	0.125
			0.40	1.11	0.448	0.372
			0.80	1.62	0.479	1.061
900	3,719	1.74	0.00	0.00	0.377	0.000
			0.20	0.65	0.467	0.133
			0.40	1.07	0.545	0.471
			0.80	1.57	0.642	1.164
1,200	4,706	1.70	0.00	0.00	0.407	0.000
			0.20	0.62	0.522	0.156
			0.40	1.03	0.612	0.498
			0.80	1.53	0.709	1.227

$$\varepsilon_s^f = c_3 \left(\frac{p}{p_a}\right)^{n_3} \left(\frac{\eta}{M_f - \eta}\right)^{n_4} \tag{10b}$$

where c_i ($i = 1$–3) and n_i ($i = 1$–4) = parameters. Eqs. (10*a*) and (10*b*) were devised based on a series of trial and error processes, the merit of which over previous ones is the use of stress and strain invariants and thus obedience to the so-called objectivity principle (Kolymbas 2000).

J. Geotech. Geoenviron. Eng., 2018, 144(7): 04018039

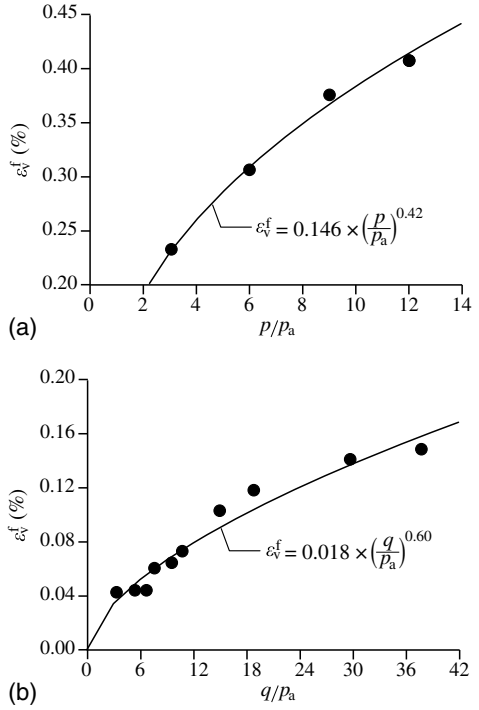

Fig. 7. Calibration of the volumetric creep strain parameters: (a) ε_v^f versus (p/p_a); and (b) ε_v^f versus (q/p_a).

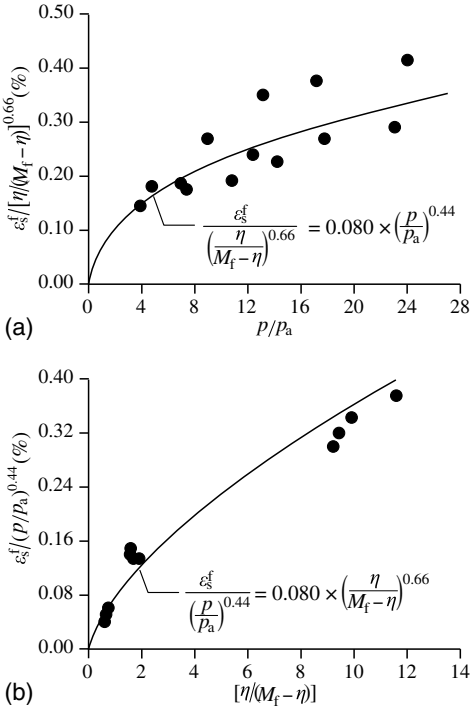

Fig. 8. Calibration of the deviatoric creep strain parameters: (a) $\varepsilon_v^f/[\eta/(M_f-\eta)^{n_4}]$ versus (p/p_a); and (b) $\varepsilon_v^f/(p/p_a)^{n_3}$ versus $[\eta/(M_f-\eta)]$.

Calibration of the parameters for the volumetric strain is relatively easy. The data obtained under isotropic stress states $(q=0)$ can be plotted on the ε_v^f versus (p/p_a) plane, and a power function best fitting the data immediately gives the values of c_1 and n_1, as illustrated in Fig. 7(a). The contributions of the first term can then be subtracted from the total volumetric strains obtained under anisotropic stress states, and the remaining amounts can be plotted similarly against (q/p_a) as shown in Fig. 7(b). Best-fitting the data points yields the values of c_2 and n_2.

To determine the parameters for the deviatoric strain, Eq. (10*b*) can be rewritten in an additive form

$$\ln \varepsilon_s^f = \ln c_3 + n_3 \ln\left(\frac{p}{p_a}\right) + n_4 \ln\left(\frac{\eta}{M_f-\eta}\right) \tag{11}$$

A linear approximation of the experimental data in the three-dimensional logarithmic space, i.e., $\ln(p/p_a)$ versus $\ln(\eta/M_f-\eta)$ versus $\ln(\varepsilon_s^f)$, using the least-squares method gives all three parameters (c_3, n_3, and n_4) once and for all. Many software packages can perform such a three-dimensional data-fitting efficiently, such as MATLAB and Mathematica. Afterward, data scatterness can be checked in sequence as demonstrated in Fig. 8. In the current case, moderate scatterness can be observed after normalizing ε_s^f by using the calibrated parameters.

For some engineering problems, the final creep strains of used materials should be evaluated. For example, the potential loss of free board during long-term operation is a critical factor to be considered in designing the crest elevation of a rockfill dam (Zhou et al. 2011). For such problems, Eqs. (10*a*) and (10*b*) and the relevant experiments and the calibration methods provide a simple way to evaluate the creep-induced deformation, as demonstrated by Zhang et al. (2004) and Zhou et al. (2011). Table 3 summarizes the seven parameters for the final amounts of creep strains of the tested rockfill material.

Table 3. Parameters for the final creep strain amounts

Parameter	Value
c_1 (%)	0.146
n_1	0.42
c_2 (%)	0.018
n_2	0.60
c_3 (%)	0.080
n_3	0.44
n_4	0.66

Time Histories of Creep Strains

The volumetric strain and deviatoric strain measured under the confining pressure of 0.6 MPa were normalized by their final amounts, and they were plotted against the logarithm of elapsed time in Fig. 9. It can be seen that the evolution of the normalized volumetric strain under different anisotropic stress states does not deviate too much from those obtained under isotropic stress states, and after a certain period of initial creeping, all $\varepsilon_v^p/\varepsilon_v^f$ versus $\log(t)$ curves can be approximated by straight lines satisfactorily. The curves plotted in Fig. 9(b), on the other hand, show more evident scatterness due to the abrupt increases of the deviatoric strains at the initial stages, as mentioned previously. Nevertheless, linear relationships also exist for the deviatoric creep strains and the logarithm of time after a certain period (generally 10 h) in most cases.

When linear strain–log time relationships were used, the secondary compressibility indices can be defined for the volumetric strain and the deviatoric strain (Augustesen et al. 2004; Liingaard et al. 2004; Oldecop and Alonso 2007), respectively

$$\lambda_v = \frac{d\varepsilon_v^p}{d(\ln t)} \tag{12a}$$

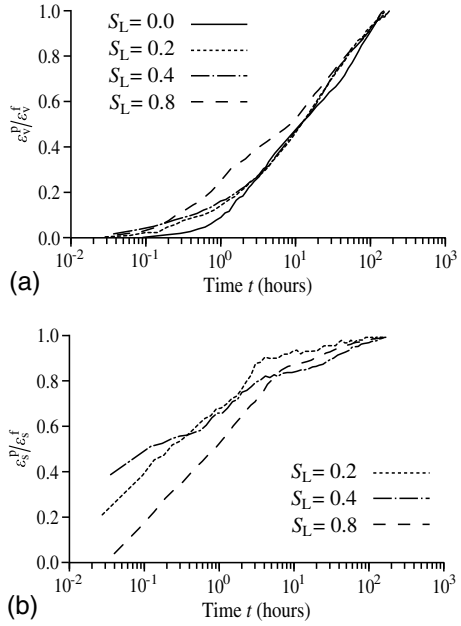

Fig. 9. Time histories of volumetric and deviatoric creep strains ($\sigma_3 = 600$ kPa): (a) ($\varepsilon_v^p/\varepsilon_v^f$) versus log t; and (b) ($\varepsilon_s^p/\varepsilon_s^f$) versus log t.

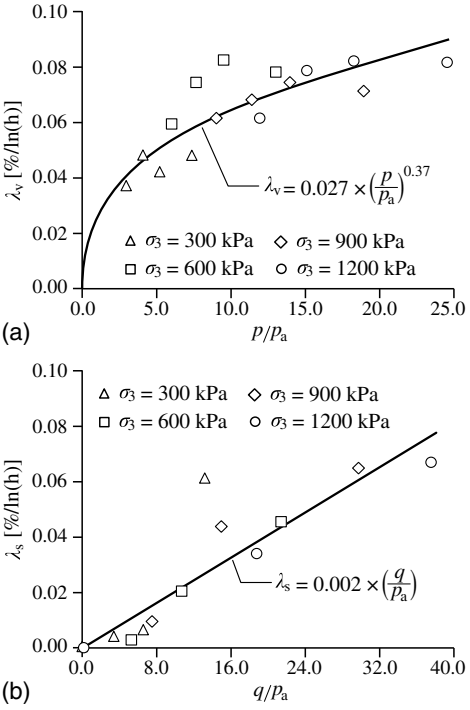

Fig. 10. Relationships between secondary compressibility indices and stress states: (a) λ_v versus (p/p_a); and (b) λ_s versus (q/p_a).

$$\lambda_s = \frac{d\varepsilon_s^p}{d(\ln t)} \tag{12b}$$

where λ_v and λ_s = proportionality constants for volumetric strain and deviatoric strain, respectively. Values of λ_v and λ_s were evaluated using experimental data from 10 h to the end of experiments, and λ_v was plotted against the mean effective stress whereas λ_s was plotted against the deviatoric stress in Fig. 10. Both λ_v and λ_s increase with the stresses: λ_v increases nonlinearly with the normalized mean effective stress, whereas λ_s shows a roughly linear dependence on the normalized deviatoric stress. Oldecop and Alonso (2007) also found a linear increase of the secondary compressibility index with the vertical stresses in suction-controlled oedometric compression experiments, and a framework rooted on the phenomenon of crack propagation in rock particles induced by stress corrosion mechanism was adopted to explain the results. Fig. 10 indicates that λ_v and λ_s can be evaluated using the following power functions:

$$\lambda_v = \lambda_{v0}\left(\frac{p}{p_a}\right)^{n_v} \tag{13a}$$

$$\lambda_s = \lambda_{s0}\left(\frac{q}{p_a}\right)^{n_s} \tag{13b}$$

where λ_{v0}, n_v, λ_{s0}, and n_s = fitting parameters. In the current case, $\lambda_{v0} = 0.027$, $n_v = 0.37$, $\lambda_{s0} = 0.002$, and $n_s = 1.0$ as shown in Fig. 10.

The results shown in Figs. 6 and 10 prove that the stress states not only have an effect on the final amounts of creep strains, but also control the rates of creep strains, similar to the findings by others (Cheng and Ding 2004; Kwok and Bolton 2013; Oldecop and Alonso 2007). In addition, the linear relationships between the creep strains and logarithm of time are in qualitative agreement with field settlement observations (Clements 1984; Oldecop and Alonso 2007). However, it deserves mention that the time scale in experiments is considerably smaller than that in field. Creep experiments in the current study generally lasted 7–10 days. Field settlement, on the other hand, often lasts several months or years depending on the compaction efforts. Therefore, the linear relations established in creep experiments only have a qualitative meaning. They cannot be used to predict the field performance quantitatively. Anyway, no matter what advanced testing system is used, the real-world field environment, such as seasonal variations of rainfall, moisture content, and temperature, is almost nonreplicable. Nevertheless, large-scale creep experiments under controlled and simplified conditions such as the work described herein do add some useful insight to the long-term behavior of both rockfill materials and rockfill dams.

Conclusions

Large-scale triaxial compression and creep experiments were performed with a typical crushed rockfill material using a creep testing apparatus. The stress dilatancy characteristics during shearing and creeping were studied. The total amounts of creep strains at the end of experiments as well as their evolution with time were also investigated. The main findings obtained from the experiments can be summarized as follows:

- Shearing a rockfill material under a constant confining pressure results in plastic volumetric contraction followed by subsequent dilation. The trend in positive dilatancy stages cannot be reproduced by the linear stress dilatancy equation used in the Cam-clay model and the nonlinear one used in the modified Cam-clay model. A nonlinear power function, with a power index of 4, was found to be a good approximation.
- Under all the stress states selected for experiments, the average creep dilatancy ratio is considerably higher than the loading-induced dilatancy ratio under the same stress states, particularly when the stress ratio is relatively low. That is to say, the material is much more contractive during creeping than during loading. The average creep dilatancy ratio decreases with the increase of

the stress ratio, following approximately the trend predicted by the nonlinear equation used in the modified Cam-clay model.
- The final amounts of creep strains at the end of experiments depend on the stress states. For a given confining pressure, a higher deviatoric stress results in a larger volumetric creep strain and also a larger deviatoric creep strain. The final amounts of creep strains also increase when the confining pressure is increased for a given stress level.
- Both the volumetric strain and deviatoric strain evolves linearly with the logarithm of time after a certain period of creeping. For the tested material, the proportionality constant for the volumetric strain increases nonlinearly with the mean effective stress, whereas that for deviatoric strain increases linearly with deviatoric stress.

The more contractive behavior during creeping than during loading observed for the tested rockfill is different from the behavior of hard sands but similar to that of friable sands. This similarity may indicate that particle breakage plays a dominating role in the creep behavior of the tested material. Systematic sieve analyses may be performed after loading and creeping in future works so as to establish relationships between the amounts of creep strains and a certain breakage index. Another point deserving further study is the scale effect on creep behavior. Disturbance of specimens during creeping is relatively low due to the small amounts of creep strains, and in this circumstance, internal fabric may play a remarkable role in mechanical responses. The complex mode of creep paths observed in this study may be caused by the insufficient scaling of the material. Increasing the specimen diameter/particle diameter ratio may yield more consistent results.

Acknowledgments

This work was supported by the national Natural Science Foundation of China (NSFC) Grant Nos. 51379130 and 51679149. Financial support from the Ministry of Water Resources (MWR) Grant No. 201501035 was also greatly appreciated.

References

Alonso, E. E., S. Olivella, and N. M. Pinyol. 2005. "A review of Beliche Dam." *Géotechnique* 55 (4): 267–285. https://doi.org/10.1680/geot.2005.55.4.267.

Alonso, E. E., E. E. Romero, and E. Ortega. 2016. "Yielding of rockfill in relative humidity-controlled triaxial experiments." *Acta Geotech.* 11 (3): 455–477. https://doi.org/10.1007/s11440-016-0437-9.

Augustesen, A., M. Liingaard, and P. V. Lade. 2004. "Evaluation of time-dependent behavior of soils." *Int. J. Geomech.* 4 (3): 137–156. https://doi.org/10.1061/(ASCE)1532-3641(2004)4:3(137).

Been, K., and M. Jefferies. 2004. "Stress-dilatancy in very loose sand." *Can. Geotech. J.* 41 (5): 972–989. https://doi.org/10.1139/t04-038.

Charles, J. A., and K. S. Watts. 1980. "The influence of confining pressure on the shear strength of compacted rockfill." *Géotechnique* 30 (4): 353–367. https://doi.org/10.1680/geot.1980.30.4.353.

Cheng, Z. L., and H. S. Ding. 2004. "Creep test for rockfill." [In Chinese.] *Chinese J. Geotech. Eng.* 26 (4): 473–476.

Clayton, C. R. I. 2011. "Stiffness at small strain: Research and practice." *Géotechnique* 61 (1): 5–37. https://doi.org/10.1680/geot.2011.61.1.5.

Clements, R. P. 1984. "Post-construction deformation of rockfill dams." *J. Geotech. Eng.* 110 (7): 821–840. https://doi.org/10.1061/(ASCE)0733-9410(1984)110:7(821).

Dolezalova, M., and I. Hladik. 2011. "Constitutive models for simulation of field performance of dams." *Int. J. Geomech.* 11 (6): 477–489. https://doi.org/10.1061/(ASCE)GM.1943-5622.0000039.

Frossard, E., W. Hu, C. Dano, and P. Y. Hicher. 2012. "Rockfill shear strength evaluation: A rational method based on size effects." *Géotechnique* 62 (5): 415–427. https://doi.org/10.1680/geot.10.P.079.

Fu, Z. Z., S. S. Chen, and S. H. Liu. 2012. "Hypoplastic constitutive modelling of the wetting induced creep of rockfill materials." *Sci. China Tech. Sci.* 55 (7): 2066–2082. https://doi.org/10.1007/s11431-012-4835-4.

Fu, Z. Z., S. S. Chen, and C. Peng. 2014. "Modeling cyclic behavior of rockfill materials in a framework of generalized plasticity." *Int. J. Geomech.* 14 (2): 191–204. https://doi.org/10.1061/(ASCE)GM.1943-5622.0000302.

Hu, W., C. Dano, P. Y. Hicher, J. Y. L. Touzo, F. Derkx, and E. Merliot. 2011. "Effect of sample size on the behavior of granular materials." *Geotech. Test. J.* 34 (3): 186–197. https://doi.org/10.1520/GTJ103095.

Hunter, G., and R. Fell. 2003. "Rockfill modulus and settlement of concrete face rockfill dams." *J. Geotech. Geoenviron. Eng.* 129 (10): 909–917. https://doi.org/10.1061/(ASCE)1090-0241(2003)129:10(909).

Indraratna, B., L. S. S. Wijewardena, and A. S. Balasubramaniam. 1993. "Large-scale triaxial testing of greywacke rockfill." *Géotechnique* 43 (1): 37–51. https://doi.org/10.1680/geot.1993.43.1.37.

Jardine, R. J., M. J. Symes, and J. B. Burland. 1984. "The measurement of soil stiffness in the triaxial apparatus." *Géotechnique* 34 (3): 323–340. https://doi.org/10.1680/geot.1984.34.3.323.

Karimpour, H., and P. V. Lade. 2010. "Time effects relate to crushing in sand." *J. Geotech. Geoenviron. Eng.* 136 (9): 1209–1219. https://doi.org/10.1061/(ASCE)GT.1943-5606.0000335.

Karimpour, H., and P. V. Lade. 2013. "Creep behavior in Virginia Beach sand." *Can. Geotech. J.* 50 (11): 1159–1178. https://doi.org/10.1139/cgj-2012-0467.

Kolymbas, D. 2000. *Introduction to hypoplasticity, advances in geotechnical engineering and tunneling*. Rotterdam, Netherlands: A.A. Balkema.

Kong, X. J., J. M. Liu, D. G. Zou, and H. B. Liu. 2016. "Stress-dilatancy relationship of Zipingpu gravel under cyclic loading in triaxial stress states." *Int. J. Geomech.* 16 (4): 04016001. https://doi.org/10.1061/(ASCE)GM.1943-5622.0000584.

Kuwano, R., and R. J. Jardine. 2002. "On measuring creep behaviour in granular materials through triaxial testing." *Can. Geotech. J.* 39 (5): 1061–1074. https://doi.org/10.1139/t02-059.

Kwok, C. Y., and M. D. Bolton. 2013. "DEM simulations of soil creep due to particle crushing." *Géotechnique* 63 (16): 1365–1376. https://doi.org/10.1680/geot.11.P.089.

Lade, P. V., C. D. Liggio, and J. Nam. 2009. "Strain rate, creep and stress drop-creep experiments on crushed coral sand." *J. Geotech. Geoenviron. Eng.* 135 (7): 941–953. https://doi.org/10.1061/(ASCE)GT.1943-5606.0000067.

Lade, P. V., and C. T. Liu. 1998. "Experimental study of drained creep behavior of sand." *J. Eng. Mech.* 124 (8): 912–920. https://doi.org/10.1061/(ASCE)0733-9399(1998)124:8(912).

Li, X. S., and Y. F. Dafalias. 2000. "Dilatancy for cohesionless soils." *Géotechnique* 50 (4): 449–460. https://doi.org/10.1680/geot.2000.50.4.449.

Liingaard, M., A. Augustesen, and P. V. Lade. 2004. "Characterization of models for time-dependent behavior of soils." *Int. J. Geomech.* 4 (3): 157–177. https://doi.org/10.1061/(ASCE)1532-3641(2004)4:3(157).

Marachi, N. D. 1969. "Strength and deformation characteristics of rockfill materials." Ph.D. thesis, Univ. of California.

Mitchell, J. M., and K. Soga. 2014. *Fundamentals of soil behavior*. 3rd ed. New Delhi, India: Wiley.

Oldecop, L. A., and E. E. Alonso. 2001. "A model for rockfill compressibility." *Géotechnique* 51 (2): 127–139. https://doi.org/10.1680/geot.2001.51.2.127.

Oldecop, L. A., and E. E. Alonso. 2007. "Theoretical investigation of the time-dependent behaviour of rockfill." *Géotechnique* 57 (3): 289–301. https://doi.org/10.1680/geot.2007.57.3.289.

Ovalle, C., C. Dano, P. Y. Hicher, and M. Cisternas. 2015. "Experimental framework for evaluating the mechanical behavior of dry and wet crushable granular materials based on the particle breakage ratio." *Can. Geotech. J.* 52 (5): 587–598. https://doi.org/10.1139/cgj-2014-0079.

Pradhan, T. B. S., F. Tatsuoka, and Y. Sato. 1989. "Experimental stress-dilatancy relations of sand subjected to cyclic loading." *Soils Found.* 29 (1): 45–64. https://doi.org/10.3208/sandf1972.29.45.

Rosco, K. H., and J. B. Burland. 1968. "On generalized stress strain behavior of wet clay." In *Engineering plasticity*, edited by J. Heyman and F. A. Leckie, 535–609. Cambridge, UK: Cambridge University Press.

Schofiled, A., and P. Wroth. 1968. *Critical state soil mechanics*. London: McGraw-Hill.

Scholey, G. K., J. D. Frost, D. C. F. Presti, and M. Jamiolkowski. 1995. "A review of instrumentation for measuring small strains during triaxial testing of soil specimens." *Geotech. Test. J.* 18 (2): 137–156. https://doi.org/10.1520/GTJ10318J.

Tapias, M., E. E. Alonso, and J. Gili. 2015. "A particle model for rockfill behavior." *Géotechnique* 65 (12): 975–994. https://doi.org/10.1680/jgeot.14.P.170.

Varadarajan, A., K. G. Sharma, K. Venkatachalam, and A. K. Gupta. 2003. "Testing and modeling two rockfill materials." *J Geotech. Geoenviron. Eng.* 129 (3): 206–218. https://doi.org/10.1061/(ASCE)1090-0241(2003)129:3(206).

Xiao, Y., H. L. Liu, Y. M. Chen, and J. Chu. 2014a. "Influence of intermediate principal stress on the strength and dilatancy behavior of rockfill material." *J. Geotech. Geoenviron. Eng.* 140 (11): 04014064. https://doi.org/10.1061/(ASCE)GT.1943-5606.0001178.

Xiao, Y., H. L. Liu, Y. M. Chen, and J. S. Jiang. 2014b. "Strength and deformation of rockfill material based on large-scale triaxial compression tests. I: Influences of density and pressure." *J. Geotech. Geoenviron. Eng.* 140 (12): 04014070. https://doi.org/10.1061/(ASCE)GT.1943-5606.0001176.

Xiao, Y., H. L. Liu, Y. M. Chen, and W. G. Zhang. 2014c. "Particle size effects in granular soils under true triaxial conditions." *Géotechnique* 64 (8): 667–672. https://doi.org/10.1680/geot.14.T.002.

Xiao, Y., H. L. Liu, Y. M. Chen, and W. G. Zhang. 2016a. "Strength and dilatancy behavior of dense modeled rockfill material in general stress space." *Int. J. Geomech.* 16 (5): 04016015. https://doi.org/10.1061/(ASCE)GM.1943-5622.0000645.

Xiao, Y., H. L. Liu, C. S. Desai, Y. F. Sun, and H. Liu. 2016b. "Effect of intermediate principal stress ratio on particle breakage of rockfill material." *J Geotech. Geoenviron. Eng.* 142 (4): 06015017. https://doi.org/10.1061/(ASCE)GT.1943-5606.0001433.

Yasuda, N., and N. Matsumoto. 1994. "Comparisons of deformation characteristics of rockfill materials using monotonic and cyclic loading laboratory tests and in situ tests." *Can. Geotech. J.* 31 (2): 162–174. https://doi.org/10.1139/t94-022.

Zhang, B. Y., T. Chen, C. Peng, X. X. Qian, and Y. X. Jie. 2017. "Experimental study on loading-creep coupling effect in rockfill material." *Int. J. Geomech.* 17 (9): 04017059. https://doi.org/10.1061/(ASCE)GM.1943-5622.0000938.

Zhang, B. Y., J. G. Wang, and R. F. Shi. 2004. "Time-dependent deformation in high concrete-faced rockfill dam and separation between concrete face slab and cushion layer." *Comp. Geotech.* 31 (7): 559–573. https://doi.org/10.1016/j.compgeo.2004.07.004.

Zhou, W., J. J. Hua, and X. L. Chang. 2011. "Settlement analysis of the Shuibuya concrete-face rockfill dam." *Comp. Geotech.* 38 (2): 269–280. https://doi.org/10.1016/j.compgeo.2010.10.004.